Article

Thermal annealing effect on the structure, optical and electrical properties of Lanthanum manganite thin films prepared by reactive co-sputtering

Wael Hourani[1]*, Christophe Rousselot[1], K.B. Joël-Igor N'Djoré[1], Alain Billard[1], Mohammad Arab Pour Yazdi[1,2] and Younes Makoudi[1]*

[1] Institut FEMTO-ST (CNRS/UFC/ENSMM/UTBM), Univ. Bourgogne Franche-Comté, Département MN2S, Place THARRADIN, F-25211 Montbéliard cedex, France

[2] Anton Paar TriTec SA, Les Vernets 6, 2035 Corcelles, Switzerland

* Correspondence: younes.makoudi@univ-fcomte.fr and wael.hourani@univ-fcomte.fr; Tel.: (+33) 381 994 681

Abstract: Lanthanum manganite (LMO) thin films were deposited by co-sputtering of La and Mn targets in Ar and O_2 gas mixture. The films were synthesized on silicon and fused silica substrates. The influences of thermal annealing on the structure, optical and electrical properties of LMO films were investigated. The results exhibited a correlation between these properties. In the amorphous state, an increase in annealing temperature improved the optical transmission and decreased the electrical capacitance. The beginning of crystallization at 600°C was manifested by a strong increase in the capacitance and a decrease in the optical transmission. At higher annealing temperature, polycrystalline films were obtained with different optical and electrical characteristics. On the other hand, the annealed LMO films showed a photocurrent effect during exposure to a weak LED light.

Keywords: Lanthanum manganite; Perovskite materials; reactive co-sputtering; capacitance meter; photocurrent

1. Introduction

Perovskite materials are a real gold mine for materials science. They are functional compounds with tailor-made characteristics [1,2,3]. Indeed, these materials have shown very rich phase diagrams and a great ability to absorb strong nonstoichiometric effects allowing to modulate, among others, their electronic, magnetic and optical properties [4,5].

Moreover, depending on their chemical compositions and crystallographic structures, these materials can be considered as a superconducting material at relatively high temperatures [6], convert heat or mechanical pressure into an electric current [7], accelerate chemical reactions or even produce an electric current by exposing them to light [8,9].

Therefore, perovskite materials have promising properties for many technological applications such as modern electronics (memories, capacitors, ultrafast electronics...), fuel cells and transparent ceramics, or photovoltaic cells [10,11].

These perovskite materials can be organic, inorganic or hybrid. The methods of their elaboration are also diverse and depend on the targeted properties, the production cost and the expected applications [12]. In the photovoltaic field, the chemical method is the dominant method for the deposition of thin layers of these materials. The organic and hybrid varieties are the most studied in the literature. In fact, the development of solar cells containing hybrid or organic perovskites as light-absorbing material has been extremely fast and has allowed to reach record yields, competing with the records of silicon-based solar cells. This success is due to the fact that hybrid perovskites have remarkable optical and electronic properties, combining the advantages of organic and inorganic semiconductors. Although these choices are motivated by the ease, the speed and the cost of the elaboration, nevertheless the stability of the films as well as the toxicity of certain elements used remain weak points of this strategy [13].

The use of inorganic materials remains a solution to circumvent these problems. Especially, as it is easier to control the stoichiometry or non-stoichiometry of these compounds prepared in vacuum. This non-stoichiometry, for example, can be important to improve the optical, magnetic and electrical characteristics of perovskite materials [14,15]

Among inorganic materials for photovoltaic application, we find materials based on lanthanum and manganese mainly prepared by chemical means [16,17,18]. However, the perovskite structure is generally preferred to obtain the best performances and especially the electrical efficiency. Indeed, in addition to the good mobility of electrical charges [19], perovskite structure has other advantages such as a good absorption of light [20].

The current study can be considered a part of this field and consists of studying lanthanum manganite thin films deposited by reactive magnetron co-sputtering process. The objective of this study is to understand how the induced perovskite structuring by annealing can contribute in the evolution of the structural, optical and electrical properties of this oxide.

A singularity of this work, lies in the choice of the stoichiometry of the LMO films and the use of simple analytical techniques, especially the capacitance meter with mercury probe in order to study the LMO film electrical properties (capacitance, photocurrent). Indeed, we made the choice to deposit slightly more Mn than La in order to evaluate the effect of probable induced lanthanum and/or oxygen deficiencies in the film on the different characteristics mentioned above.

2. Experiments

LMO thin films were deposited by co-sputtering of La (purity 99.9 at.%, diameter 50 mm, thickness 3 mm) and Mn (purity 99.9 at.%, diameter 50 mm, thickness 3 mm) targets in Ar and O_2 gas mixture. Such a deposition technique easily allowed us to vary the stoichiometry ratio La/Mn by changing discharge power on both targets. The sputtering reactor is a 90 L cylinder Alcatel 604 SCM pumped down via a turbomolecular pump system that allows a residual vacuum below 10^{-4} Pa. Ar and O_2 gas flow rates were controlled with Brooks flowmeters with $Q_{Ar} = 50$ sccm and $Q_{O2} = 20$ sccm, respectively. The total pressure ($P_{tot} = 0.45$ Pa) was measured with a Baratron manometer from MKS Instruments. N-doped silicon (orientation (111), phosphorus doped, 2x2 cm^2) as well as fused silica slide (2x2 cm^2) were used as substrates. Before each deposit, all our substrates have been cleaned with ethanol. The fused silica samples were additionally washed with soap and water. The rotating substrate holder was parallel to La and Mn sources at a distance of about 60 mm and all depositions were carried out at floating temperature ($T_{substrate} < 70$ °C).

The La and Mn targets were supplied with a pulsed DC (Direct Current) Advanced Energy dual generator allowing the control of the discharge power. The discharge currents of La and Mn were fixed to 0.5 A and 0.34 A respectively. The discharge power was changed on both targets to adjust the film composition. The principal parameters used for the elaboration of our films are summarized in the table below.

***Table 1.** Films deposition parameters.*

Target	Discharge Power (W)	Frequency (kHz)	T_{off} (µs)	Ar Flow Rate (sccm)	Working Pressure (Pa)	Run Duration (min)	Draw Distance (DT-S) (mm)	Discharge Current (A)
La	82-128	50	4	50	0.45	12	60	0.5
Mn	100-105	70						0.34

After the synthesis of the film with the desired composition, annealing at different temperatures (400 °C, 500 °C, 600 °C and 700 °C) of the sample for 3 hours is performed in the furnace under air. After each annealing, the structural, optical and electrical properties of the film were studied.

The chemical composition was performed by Energy Dispersive X-ray Spectroscopy (EDS, Bruker nano, Berlin, Germany). These measurements were performed on the sample before annealing. The film's thickness was measured by step method with an Altisurf Profilometer (Altisurf 500) manufactured by Altimet society. Before each measurement, the calibration of the experimental device was realized with a reference sample number 787569 accredited by CETIM organization.

The structural characterization of coatings was performed by Bragg-Brentano configuration X-ray diffraction (XRD) using a BRUKER D8 focus diffractometer (Bruker AXS, Karlsruhe, Germany) with a cobalt X-ray tube (Co $K\alpha_1+\alpha_2$ radiations λ = 0.178897 nm) and equipped with a LynxEye linear detector.

Diffractograms were collected in air in the angle range 20°-80° at a scan speed (2θ) of 0.1/s.

The evolution of the optical transmission as a function of the wavelength (200-1500 nm) was measured using a Lambda 950 spectrophotometer from Perkin Elmer. The determination of the optical gap of the film is deduced from the Tauc relation [21].

LMO thin film electrical properties were measured with the MDC 802C mercury probe capacitance meter (Materials Development Corporation). Only the film deposited on silicon has been characterized. The MOS (Metal Oxide Semiconductor) structure is mandatory for these measurements. Our film is therefore considered as an oxide. The operation of this tool is as follows: the sample to be characterized is placed on the support, upside down, i.e. the film to be characterized is at the bottom. The lever is lowered to be in contact with the silicon at the back of the sample. A drop of mercury rises through a capillary and comes into contact with the film to be characterized. The surface of the drop-in contact with the film is very precisely controlled, and is 4.72 x 10^{-3} cm^2. This probe is connected to an Agilent 4284A impedance analyzer. This device measures the complex impedance of the structure when subjected to a sinusoidal bias of the form $U(t) = V_g(t) + s(t)$ with $s(t) = S_0 \sin(\omega t)$. The gate bias voltage $V_g(t)$, which varies in steps so that each measurement point is obtained at thermodynamic equilibrium, allows to probe the different operating regimes of the structure (accumulation, depletion and inversion). The small sinusoidal signal s(t) allows to extract the differential capacity and thus C_{tot} versus V_g, named C-V curve. The flat band voltage V_{FB} can be deduced from the C-V curve by using the flat band capacitance (C_{FB}) method [22]. With this method, the ideal C_{FB} value is calculated from the film capacitance and the Debye length. After the value of C_{FB} is known, the value of V_{FB} can be deduced from the C-V curve data, by interpolating between the closest V_g values. More details on this technique can be found in previous paper [23].

A simple LED lamp (from PREVAC, 1W power) was introduced under the sample to evaluate the photoelectric effect of the film (see Figure 1). Only the sample side with the deposition was illuminated. The operation consists of measuring the current over a specific time in the dark (closed box during 1 minute) and under illumination (closed box + LED light during 2 minutes) and in dark again during 1 minute. The sample was polarized at -2 V during the measurements. This voltage is applied in order to create the electric field that will separate the electron-hole pair generated by the light in the film.

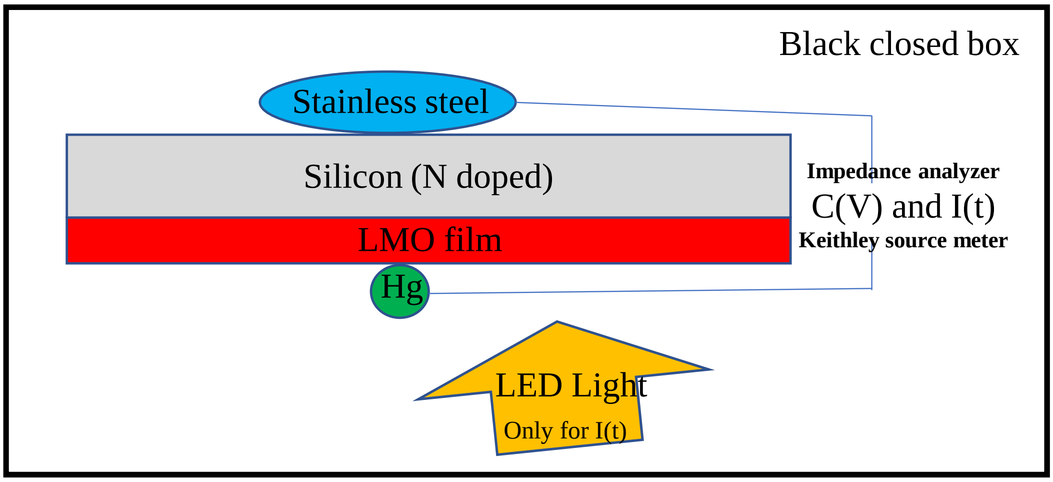

Figure 1. *A schematic diagram of the experimental setup of the capacitance meter with a mercury probe.*

3. Results

The thickness of the studied films is measured to be 375 nm. The EDS elemental spectra of LMO film confirms the presence of La and Mn elements in the film with atomic percentage measured to be 48 % and 52 % respectively.

Figure 2 shows the XRD patterns of the LMO film versus annealing temperature. The as deposited film was amorphous and after annealing at 400 °C and 500 °C, no significant peaks were detected. The film crystallization started at 600 °C, with a small diffraction peak at 38.22°. Other smaller peaks of lower intensity were also observed at 26.73°, 30.76°, 47.46° and 55.02° angles. Finally, after annealing at 700 °C the peak at 30.76° was vanished while the intensity of the other peaks increased and two new peaks (62.35° and 69.23°) were appeared.

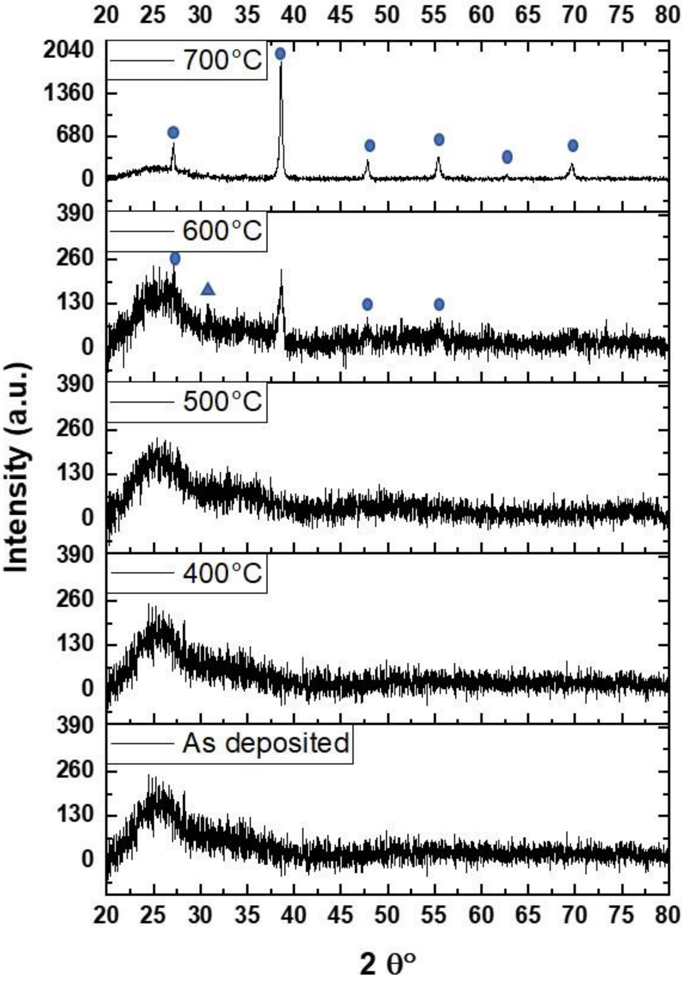

Figure 2. XRD spectra of the LMO film as deposited and after annealing (400°C, 500°C, 600°C and 700°C). The peaks indicated by the circles represent the perovskite structure $La_{0.887}MnO_3$ and the triangle indicates the Mn_3O_4 phase. .

The optical spectra of Figure 3(a) show that the transmission increased after annealing at 400 and 500 °C. The film transmittance then decreased after annealing at 600°C, and finally the film transmittance decreased drastically after annealing at 700°C. From the transmittance drop region, we deduced the optical gap of each measurement. The latter is estimated from the intersection of the extrapolation of the curve giving $(\alpha h\upsilon)^{0.5} = f\ (h\upsilon)$ with the x-axis [21] (see Figure 3(b)), where α is the absorption coefficient which can be calculated using the following formula : $\frac{1}{Thickness} ln\left(\frac{1}{Transmission}\right)$, h is Planck constant and ν is the light's frequency. It was 1.74 eV before annealing then 1.93 eV after annealing at 400°C, 500°C and 600°C. However, after annealing at 700°C the film was so opaque that it was impossible to determine the optical gap (<< 1 eV).

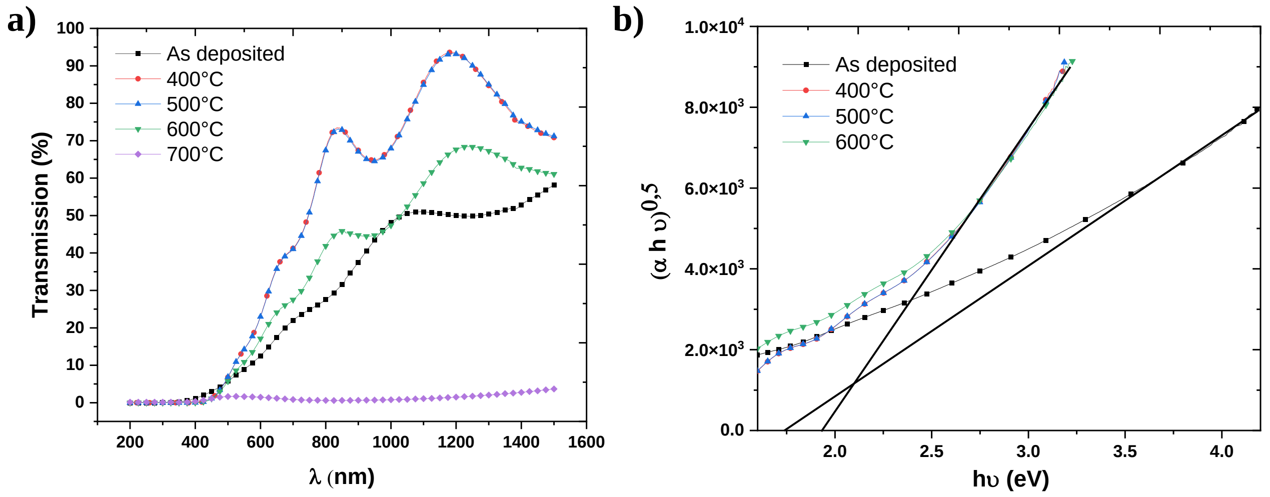

Figure 3. : (a) Transmission spectra of the LMO film as deposited and after annealing (400°C, 500°C, 600°C and 700°C). (b) Determination of the optical gap.

Figure 4(a) shows the capacitance measurements obtained before and after the different annealing processes. The dielectric constants (K), calculated from the maximum value of C_{ox} in accumulation, of each measurement are also displayed. The shape of the curves is almost identical and some evolutions are noted (Figure 4(b)). First, the value of the dielectric constant (red curve) decreased after the first annealing at 400°C (from K = 21 to K = 14), remained almost stable after the second annealing at about 500 °C (K = 13) then increased strongly after annealing at 600 °C (K = 30) to finally drop after the last annealing at 700°C (K = 7). Secondly, the flat band voltage V_{FB} (black curve) increases strongly after the annealing at 400°C. Then, it decreases after the annealing at 500°C and 600°C. Finally, after annealing at 700°C, V_{FB} rises again. The variation of V_{FB}, is reflected by a shift of the C (V) curves to the right, as it is the case after annealing at 400°C and 700°C, or to the left after annealing at 500 and 600°C

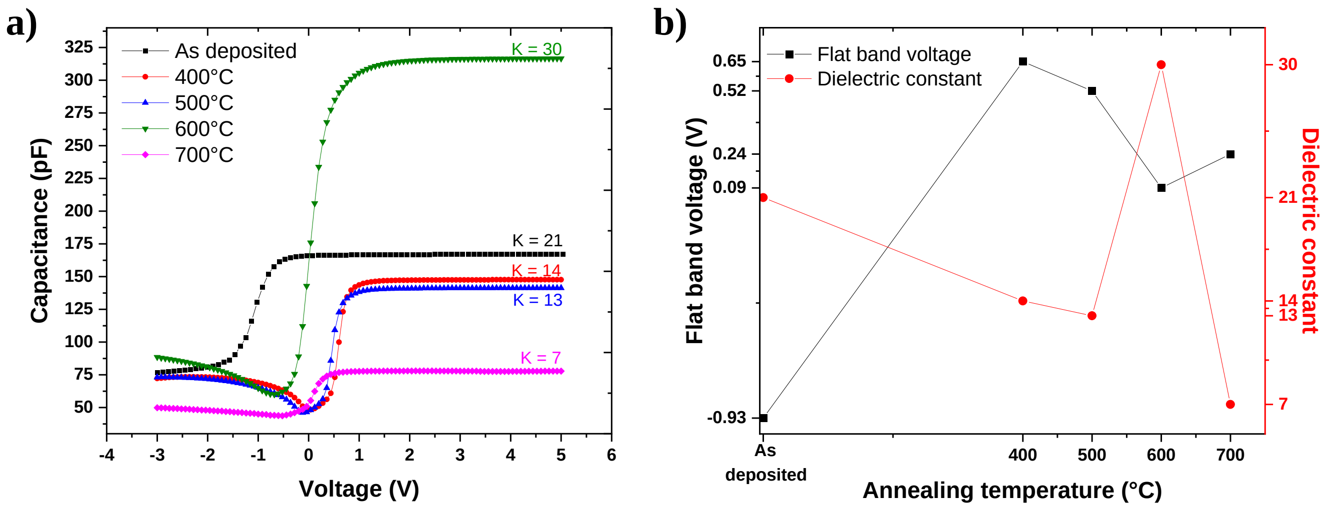

Figure 4. (a) C-V characteristics curves at 1 MHz of Hg-LMO-Si MOS structures obtained for the LMO film as deposited and after annealing with the values of the relative dielectric constants K. (b)

Flat band voltage V_{FB} (black curve) and dielectric constant (red curve) in function of different annealing temperatures.

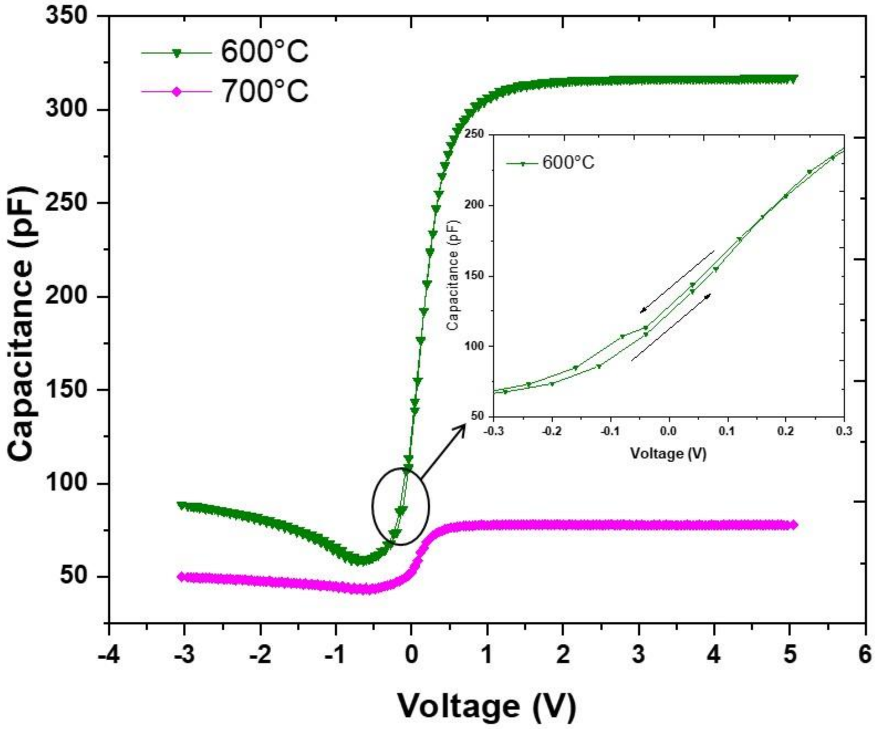

Figure 5. Capacitance-voltage hysteresis measurements at 1 MHz of the LMO film after annealing at 600 and 700°C respectively. Inset: zoom-in on the C-V of the LMO film after 600°C showing the small hysteresis loop.

Figure 5 shows the measured *C–V* hysteresis characteristics of the LMO film after annealing at 600 and 700 °C. A zoom is performed to appreciate the extent of the hysteresis. A small dip (marked with a rectangle in Figure 5) in the weak inversion region of the C–V curves is visible. This behavior only concerns the curve obtained at 600°C and disappears after annealing at 700°C.

The exposure of the film to LED light, although very weak, led to the generation of a photocurrent. Figure 6 shows the results obtained after annealing at 600°C and 700°C. We observe that the current through the film is almost stable at the beginning in the dark. This electric current represents the leakage current in the material and it is measured in function of the illuminated surface (i.e. sample size of 4 cm^2). When the LED is turned on, the current increases and then returns to its initial value by turning off the light. One evolution is noticed after the annealing at 700°C. The value of the current in darkness increased from about -0.03 $\mu A/cm^2$ to -0.06 $\mu A/cm^2$. On the other hand, the variation of the current induced by the light seems to be the same, approximately 2.5 nA/cm^2.

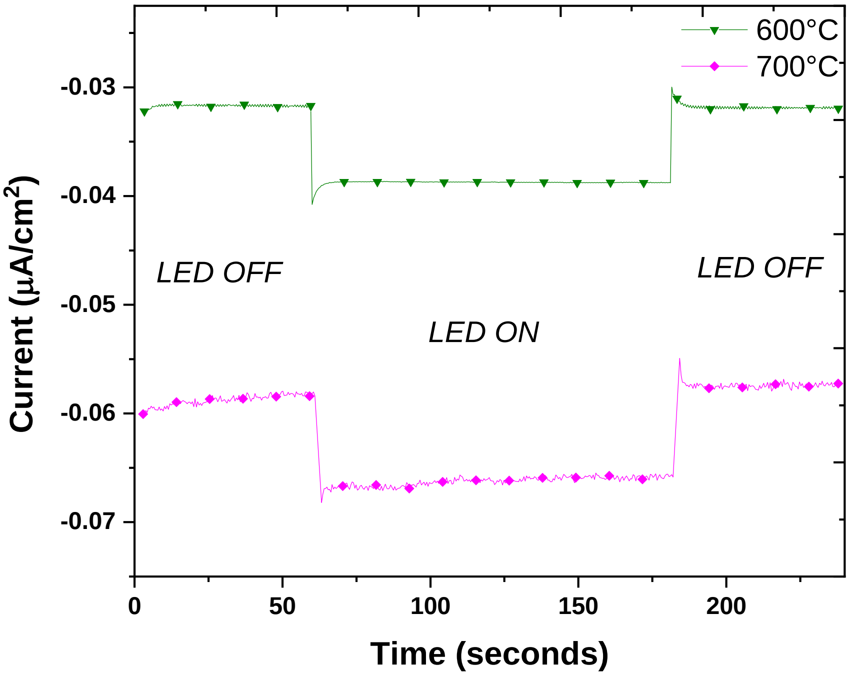

Figure 6. Current-time measurements obtained with an applied voltage of -2V on the LMO film after annealing at 600 and 700°C and exposed or not to an LED light.

4. Discussion

Our films are all 375 nm thick. This thickness choice is justified by the objective of obtaining a good photoelectric efficiency of our LMO layer. Indeed, it is generally accepted that if the thickness of the absorbing material is very small, then there will be a weak absorption of light and consequently a weak photogeneration of excitons. On the other hand, if the film is very thick, many charge carriers recombine before leaving this material [24].

Concerning the XRD patterns of LMO films shown in Figure 2, it is possible to appreciate that the diffraction peaks agree with the $La_{0.92}MnO_3$ [25] structure. Accordingly, the peaks indicated by the circles represent the perovskite structure and the triangle indicates the Mn_3O_4 phase. These statements agree with the EDS results where La rate is slightly lower than Mn one. The peak at 2θ = 30.76° which was obtained at annealing temperature of 600 °C has disappeared after annealing at 700 °C. This observation could be explained by the transformation of the Mn_3O_4 phase into Mn_5O_8 one, even less important and poorly crystallized [26].

The transmittance increase after the film was subjected to 400°C thermal annealing could be attributed to the decrease in defects and structural relaxation of the amorphous film. The second annealing at 500°C did not change the optical transmission since the crystal structure of the film remained the same. After the third annealing at 600°C, the transmittance is decreased due to the onset of crystallization and changes in local bonding. This decrease in transmittance is even more apparent after the fourth annealing at 700°C. Indeed, the transmittance decreased due to larger scale crystallization, with the formation of a few major crystalline phases. This trend of transmittance decreasing is consistent with theoretical models based on Rayleigh-Gans-Debye theory, according to which diffusion increases and thus transmittance decreases with increasing grain size [27,28].

The drop of the optical gap translated by the drop of the transmission after the annealing at 700°C, could be explained, in addition to what was advanced before, by the amorphous-crystalline transformation as observed from the XRD data and reported elsewhere [29].

After the first and second annealing, the amorphous structure gives way to grains whose quantity increases with the annealing temperature. The dielectric loss caused by the grain boundaries is increased and consequently the dielectric constant decreased (Figure 4b). However, when the processing temperature is relatively high (600°C), the number of grains is then reduced due to the coalescence of small grains into larger poly crystal grains; and consequently, the dielectric loss is considerably reduced. This leads to an increase in the dielectric constant. Increasing the annealing temperature further (700°C) resulted in more crystallization of the film into a multitude of crystallites of various orientations and separated by a multitude of grain boundaries. This polycrystallinity could explain the drop of the dielectric constant. These results agree with what has been observed and modeled for ferroelectric (Ba,Sr)TiO3 thin films and pyrochlore-type $Pb(Mg,Nb,Ti)O_3$ dielectric films [30].

For n-type substrate, the positive shift of the flat band voltage (i.e. displacement of the C-V curve to the right) means that the film has lost positive charges. In other words, it is richer in oxygen. However, a negative shift of the C-V characteristics is caused by positive fixed charges. The change of oxidation states of the Mn transition metals or/and the creation of oxygen vacancies at the grain boundaries of the polycrystalline structure in the film, could be at the origin of this behavior. This explanation is consistent with a proven fact that oxygen deficiencies generally tend to decrease with increasing temperature [31].

Concerning the I(t) curves results, the improvement of the induced current by applying -2V to the structure in the absence of light is mainly explained by the improvement of the crystal structure of the film. We could also attribute it to an improvement of the silicon/film interface as a result of the annealing. Indeed, the small dip observed in Figure 5 would indicate that the LMO film contains interface trapped charges between the film and the silicon wafer. However, this contribution would remain low since our C-V measurements after annealing at these temperatures (600 °C and 700 °C) do not show strong hysteresis (see Figure 5). Hysteresis that we could attribute, among others, to interface defects. This improvement of the crystallinity has a negative effect on the dielectric constant which has decreased (from 30 to 7). Consequently, the film does not separate efficiently the excitons produced by the light [32]. Therefore, we have less photocurrent. This could explain the second observation. In other words, what we have gained by creating order in the material, has been lost by the decrease of the dielectric constant.

Although our light source does not correspond to what is usually used in the literature especially in terms of power, wavelength and standards [33], our first results show that LMO material could be a promising absorber material in a photovoltaic cell. These results show also that it is possible to optimize the temperature and the annealing time to improve the photocurrent.

5. Conclusions

LMO films have been deposited on silicon and fused silica substrates by co-sputtering of Lanthanum and Manganese targets in Ar and O_2 gas mixture. The effects of annealing on the structure, optical and electrical properties of LMO films are investigated.

For annealing temperatures below 600°C the film is amorphous and transparent. The amount of LMO grains during crystallization increases leading to more dielectric losses and the insertion of oxygen in the film. The annealing at 600°C marks the beginning of the crystallization of the film and the optical transmission decreases. The Mn_3O_4 and perovskite phases coexist in this case. The coalescence of the grains leads to a drop in the dielectric losses and thus a strong increase in the dielectric constant. The annealing at 700°C leads to a drastic drop of the optical transmission and of the dielectric constant. The reinforcement of the perovskite structure, the disappearance of the Mn_3O_4 phase and the improvement of the silicon/LMO interface are also observed.

The exposure of the annealed samples at 600 °C and 700°C to a very low intensity LED light leads to the production of a photocurrent. The gain obtained thanks to the crystallization and the improvement of the Si/LMO interface is counterbalanced by the fall of the dielectric constant. Therefore, the photocurrent is almost the same in both cases.

Finally, by elaborating LMO films by PVD technique we can easily control the stoichiometry. With a simple LED lamp and by using a simple characterization technique, we can generate a photo-current. This way of doing things, could give ideas to explore the other ways.

References

1- Judeinstein, P., & Sanchez, C. (1996). Hybrid organic–inorganic materials: a land of multidisciplinarity. *Journal of Materials Chemistry*, *6*(4), 511-525.

2- Saparov, B., & Mitzi, D. B. (2016). Organic–inorganic perovskites: structural versatility for functional materials design. *Chemical reviews*, *116*(7), 4558-4596.

3- Lin, G. C., Wei, Q., & Zhang, J. X. (2006). Direct measurement of the magnetocaloric effect in La0. 67Ca0. 33MnO3. *Journal of magnetism and magnetic materials*, *300*(2), 392-396.

4- Coey, J. M. D., Viret, M., & Von Molnar, S. (1999). Mixed-valence manganites. *Advances in physics*, *48*(2), 167-293.

5- Wolf, S. A., Awschalom, D. D., Buhrman, R. A., Daughton, J. M., von Molnár, V. S., Roukes, M. L., ... & Treger, D. M. (2001). Spintronics: a spin-based electronics vision for the future. *science*, *294*(5546), 1488-1495.

6- Maeno, Y., Hashimoto, H., Yoshida, K., Nishizaki, S., Fujita, T., Bednorz, J. G., & Lichtenberg, F. (1994). Superconductivity in a layered perovskite without copper. *nature*, *372*(6506), 532-534.

7- Bai, Y., Siponkoski, T., Peräntie, J., Jantunen, H., & Juuti, J. (2017). Ferroelectric, pyroelectric, and piezoelectric properties of a photovoltaic perovskite oxide. *Applied Physics Letters*, *110*(6), 063903.

8- Xu, X., Zhong, Y., & Shao, Z. (2019). Double perovskites in catalysis, electrocatalysis, and photo (electro) catalysis. *Trends in Chemistry*, *1*(4), 410-424.

9- Jodlowski, A., Rodríguez-Padrón, D., Luque, R., & de Miguel, G. (2018). Alternative perovskites for photovoltaics. *Advanced Energy Materials*, *8*(21), 1703120.

10- Sun, C., Alonso, J. A., & Bian, J. (2021). Recent advances in perovskite-type oxides for energy conversion and storage applications. *Advanced Energy Materials*, *11*(2), 2000459.

11- Ren, R., Wang, Z., Meng, X., Wang, X., Xu, C., Qiao, J., ... & Sun, K. (2020). Tailoring the oxygen vacancy to achieve fast intrinsic proton transport in a perovskite cathode for protonic ceramic fuel cells. *ACS Applied Energy Materials*, *3*(5), 4914-4922.

12- Schmidt-Mende, L., Dyakonov, V., Olthof, S., Ünlü, F., Lê, K. M. T., Mathur, S., ... & Draxl, C. (2021). Roadmap on organic–inorganic hybrid perovskite semiconductors and devices. *APL Materials*, *9*(10), 109202.

13- Rao, M. K., Sangeetha, D. N., Selvakumar, M., Sudhakar, Y. N., & Mahesha, M. G. (2021). Review on persistent challenges of perovskite solar cells' stability. *Solar Energy*, *218*, 469-491.

14- Thoutam, L. R., Yue, J., Xu, P., & Jalan, B. (2019). Hopping transport in SrTi O 3/N d 1− x Ti O 3/SrTi O 3 heterostructures. *Physical Review Materials*, *3*(6), 065006.

15- Hashimoto, T., Yamaguchi, M., Sakurai, Y., & Oikawa, E. (2008). Effect of oxygen nonstoichiometry on electrical conduction property of BaBiO3− δ. *Journal of Physics and Chemistry of Solids*, *69*(2-3), 284-288.

16- Hossain, A., Atique Ullah, A. K. M., Sarathi Guin, P., & Roy, S. (2020). An overview of La2NiMnO6 double perovskites: synthesis, structure, properties, and applications. *Journal of Sol-Gel Science and Technology*, *93*(3), 479-494.

17- Kumar, M., Raj, A., Kumar, A., & Anshul, A. (2021). Theoretical evidence of high power conversion efficiency in double perovskite solar cell device. *Optical Materials*, *111*, 110565.

18- Ibarra-Rodriguez, L. I., Garay-Rodríguez, L. F., & Torres-Martínez, L. M. (2022). Photocatalytic reduction of CO2 over LaMO3 (M: Fe, Co, Mn)/CuxO films. *Materials Science in Semiconductor Processing*, *139*, 106328.

19- Sheikh, M. S., Ghosh, D., Dutta, A., Bhattacharyya, S., & Sinha, T. P. (2017). Lead free double perovskite oxides Ln2NiMnO6 (Ln= La, Eu, Dy, Lu), a new promising material for photovoltaic application. *Materials Science and Engineering: B*, *226*, 10-17.

20- Wu, H., Si, H., Zhang, Z., Kang, Z., Wu, P., Zhou, L., ... & Zhang, Y. (2018). All-Inorganic Perovskite Quantum Dot-Monolayer MoS2 Mixed-Dimensional van der Waals Heterostructure for Ultrasensitive Photodetector. *Advanced Science*, *5*(12), 1801219.

21- J. Tauc (Ed.), Amorphous and Liquid Semiconductor, Plenum Press, New York, 1974, p. 159.

22- Schroder, D. K. (2015). *Semiconductor material and device characterization*. John Wiley & Sons.

23- N'Djoré, K. B. J. I., Grafouté, M., Makoudi, Y., Hourani, W., & Rousselot, C. (2022). Tuning the Electrical Properties of Tungsten Oxide Thin Films Deposited by Reactive Magnetron Sputtering. *Coatings*, *12*(2), 274.

24- Thankappan, A., & Thomas, S. (Eds.). (2018). *Perovskite Photovoltaics: Basic to Advanced Concepts and Implementation*. Academic Press.

25- Dezanneau, G., Sin, A., Roussel, H., Audier, M., & Vincent, H. (2003). Magnetic properties related to structure and complete composition analyses of nanocrystalline La1− xMn1− yO3 powders. *Journal of Solid State Chemistry*, *173*(1), 216-226.

26- Ulutas, C., Erken, O., Gunes, M., & Gumus, C. (2016). Effect of annealing temperature on the physical properties of Mn3O4 thin film prepared by chemical bath deposition. *Int. J. Electrochem. Sci*, *11*, 2835-2845.

27- Jin, Y., Bond, C. W., Leonard, R. L., Liu, Y., Johnson, J. A., & Petford-Long, A. K. (2021). The effect of annealing on optical transmittance and structure of ZLANI fluorozirconate glass thin films. *Micron*, *140*, 102977.

28- Wen, T. C., & Shetty, D. K. (2015). On the effect of birefringence on light transmission in polycrystalline magnesium fluoride. *Journal of the American Ceramic Society*, *98*(3), 829-837.

29- Abd-Elrahman, M. I., & Hafiz, M. M. (2013). On thickness and annealing dependence of optical properties of Te67. 5 Ga2. 5 As30 thin film as optoelectronic material. *Journal of alloys and compounds*, *551*, 562-567.

30- Zhu, X. H., Guigues, B., Defaÿ, E., & Aïd, M. (2008). Modeling of the evolution of dielectric loss with processing temperature in ferroelectric and dielectric thin oxide films. *Journal of Applied Physics*, *104*(7), 074118.

31- Jeong, W. Y., Lee, Y. H., & Farouk, B. (2003). Annealing effects on structural and electrical properties of fluorinated amorphous carbon films deposited by plasma enhanced chemical vapor deposition. *Thin solid films*, *423*(1), 97-102.

32- Su, R., Xu, Z., Wu, J., Luo, D., Hu, Q., Yang, W., ... & Zhu, R. (2021). Dielectric screening in perovskite photovoltaics. *Nature communications*, *12*(1), 1-11.

33- Sharma, V., & Chandel, S. S. (2013). Performance and degradation analysis for long term reliability of solar photovoltaic systems: A review. *Renewable and sustainable energy reviews*, *27*, 753-767.